IEEE Antennas & Propagation Magazine

Volume 50, No. 1, February 2008 www.ieeeaps.org (ISSN 1045-9243)

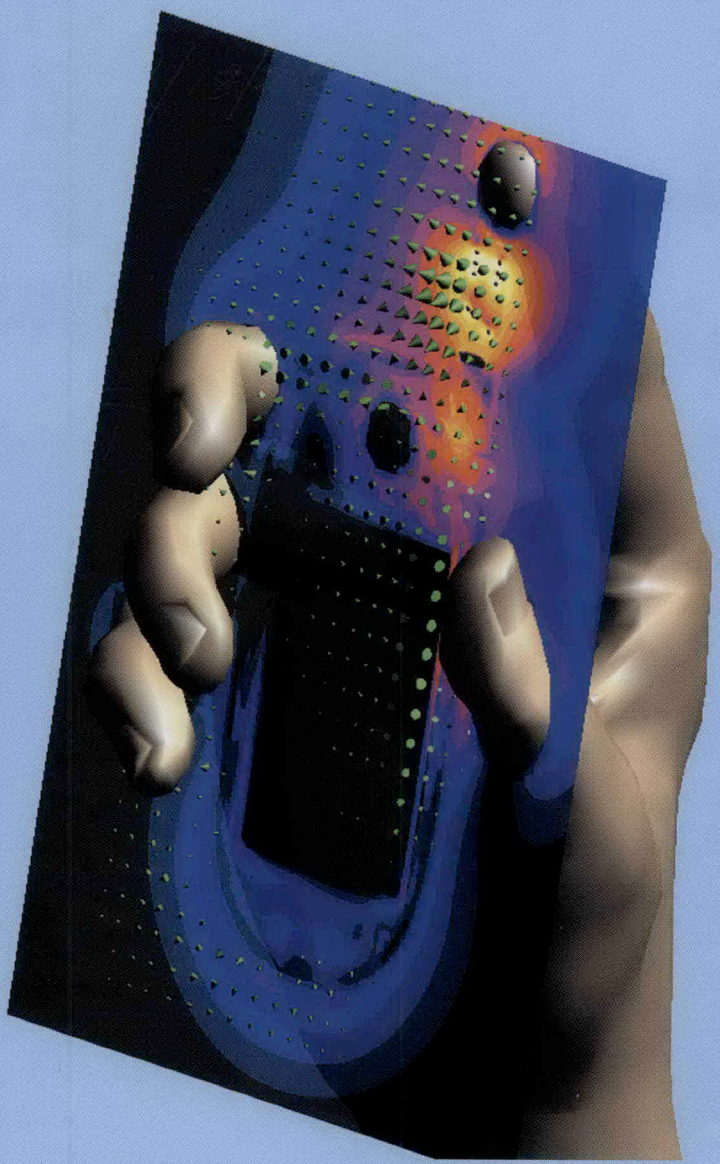

Reliable Prediction of Mobile Phone Performance for Realistic In-Use Conditions Using the FDTD Method

P. Futter[1], N. Chavannes[1], R. Tay[2], M. Meili[1], A. Klingenböck[3], K. Pokovic[1], and N. Kuster[3]

[1]Schmid & Partner Engineering AG (SPEAG), Zurich, Switzerland
E-mail: futter@speag.com

[2]Motorola Electronics Private Ltd., Singapore
[3]Foundation for Research on Information Technologies in Society (IT'IS), Zurich, Switzerland

Abstract

The objective of this study was to analyze whether advanced simulation platforms provide the effectiveness, accuracy, reliability, and efficiency to predict impairment of mobile-phone RF performance under various usage patterns. The investigation was based on the mechanical CAD data of a commercial phone with two alternative antennas. Three significant hand positions were modeled and evaluated with the device against the SAM head. The results demonstrated high reliability and suitability for providing decision rationale for the design of complex high-end multi-band mobile phones.

Keywords: FDTD methods; numerical analysis; simulation software; software tools; computer aided analysis; computer aided engineering; design automation; mobile communication; mobile antennas; antenna measurements; dosimetry; land mobile radio cellular systems

1. Introduction

Computational electromagnetics (CEM), in particular using the Finite-Difference Time-Domain Method [1] originally presented by Yee [2], has made substantial progress. A few years ago, simulations were restricted to generic phone models [3-5]. In [6], it was demonstrated for the first time that reliable prediction of the far-field and near-field quantities, including specific absorption rate (SAR), can be obtained in standardized configurations if all phone components exceeding the size of 1 mm^3 are accurately modeled. This can be rapidly achieved today by importing the mechanical CAD files.

This study was carried out during the early design phase of a mobile-phone device. Although the device exhibited good over-the-air (OTA) performance (as defined by [7]) for free-space and against-the-head loading, severe degradation of performance was recorded when the device was held in certain positions. The goals of this study were to use a CEM simulation tool to first validate the measured free-space and against-the-head performance, and secondly to reproduce the degradation of performance that occurred when the device was held in certain positions by the user. This was done by including three different hand models in the simulations and recording the performance.

2. Mobile-Phone Device

The phone used for this study was a quad-band (GSM850/900, DCS, PCS) V180 clamshell phone, manufactured by Motorola Inc., and shown in Figure 1. When the study was initiated, the phone was not yet commercially available. Highly detailed `.IGES` CAD files were provided describing the geometry of the phone, which could be directly imported into the simulation tool (Figure 1, top). Furthermore, two different antenna configurations were considered within the study. Several devices were available for measurement purposes and validation of the CAD data.

3. Numerical Method

The IT'IS Foundation, in cooperation with the Integrated Systems Laboratory of ETHZ and Schmid & Partner Engineering AG (SPEAG), has continued its efforts to improve its FDTD-based platform to obtain more-efficient, more-accurate, and easier-to-apply simulations. The latest achievements include a set of novel kernels, including FIT/CFDTD solvers [8, 9] for gridding non-conformally aligned structures of arbitrary complexity.

ISSN 1045-9243/2008/$25

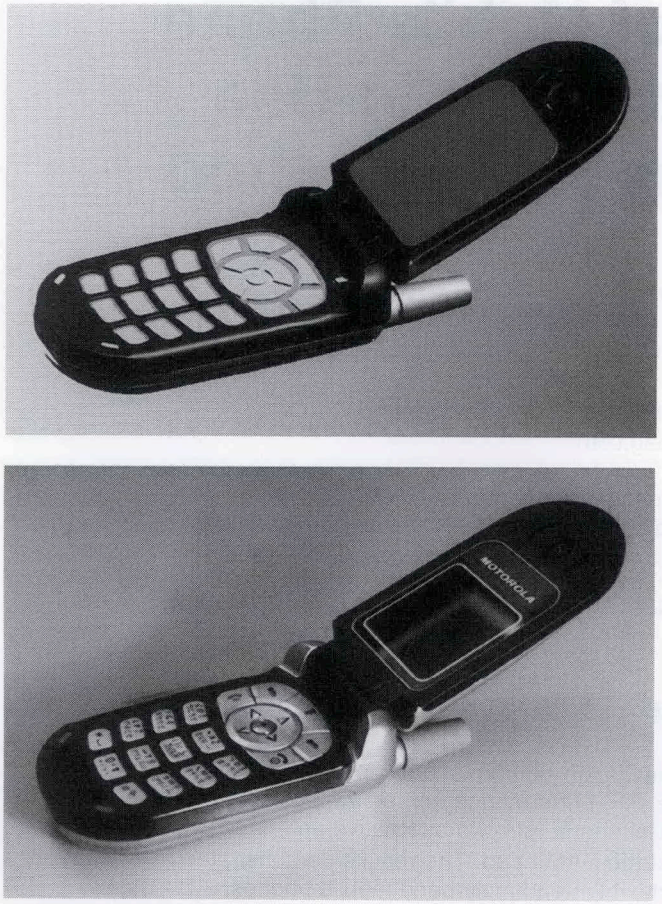

Figure 1. The multi-band phone used in this study: a photograph of the actual phone (bottom), and the CAD-derived model (top).

Furthermore, ADIFDTD [10] and FIT/C-ADI-FDTD [11] solvers can effectively compute highly over-discretized structures. A novel thermal solver [12] allows coupled EM-thermal simulations, including blood-flow modeling for CAD-based anatomical models. Integration of hardware-accelerated FDTD [13] allows for computational performance such as outlined in Section 8, and supports a novel genetic-algorithm-based optimizer derived from [14]. Enhanced FDTD grid generators and voxelers [15, 16] support all solvers and specific features, such as effective modeling of thin metallic coatings [17]. These features are currently made commercially available in the Jungfrau release of *SEMCAD X V11.0* by SPEAG [18].

4. Measurement Technique

The measurements were conducted with the near-field scanning system DASY4 of SPEAG (see Figure 2), using the appropriate near-field probes (see Table 1) and the TwinSAM phantom [19]. The probes and the system were calibrated according to [20, 21, 19], according to the requirements of ISO17025. Far-field measurements according to the requirements of [7] were carried out at Motorola Singapore.

5. FDTD Modeling

5.1 Generation of an Accurate FDTD Representation of the Phone

The CAD data describing the phone was provided by Motorola in `.IGES` format. The original model contained

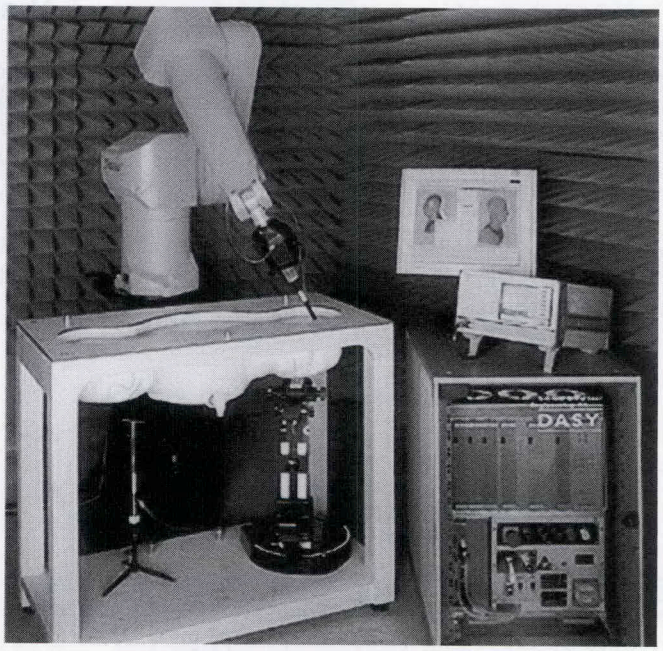

Figure 2. The automated dosimetric assessment system, DASY4: measurement of a mobile phone.

Table 1. DASY4 probes employed for the experimental evaluation. The dynamic range was equal to or larger than 0.1-3.0 GHz, and the linearity was better than ±0.2 dB for all probes.

Probe Type	Diameter [mm]	Dynamic Range	Dev. of Axial Isotropy [dB]	Dev. of Spherical Isotropy [dB]
ET3DV6 1374	6.8	2 μW-0.1 W/g	< ±0.05	< ±0.20
EF3DV2 4004	3.9	2 -1000 V/m	< ±0.05	< ±0.30
H3DV6 6060	5.0	0.01 -2 A/m	< ±0.12	< ±0.20

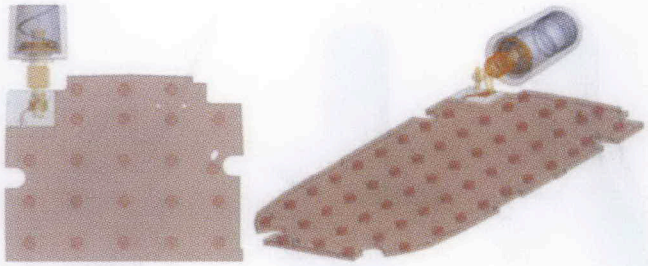

Figure 3. The antenna feed structure and the multilayer PCB configuration.

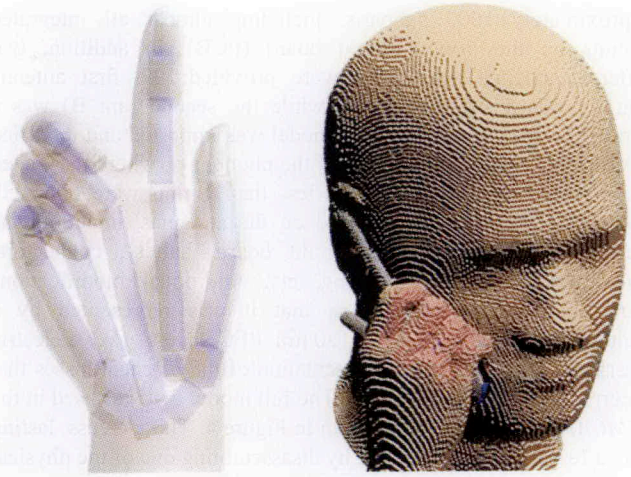

Figure 7. The non-homogeneous hand model (left), and the discretized representation of the phone, head, and hand (right).

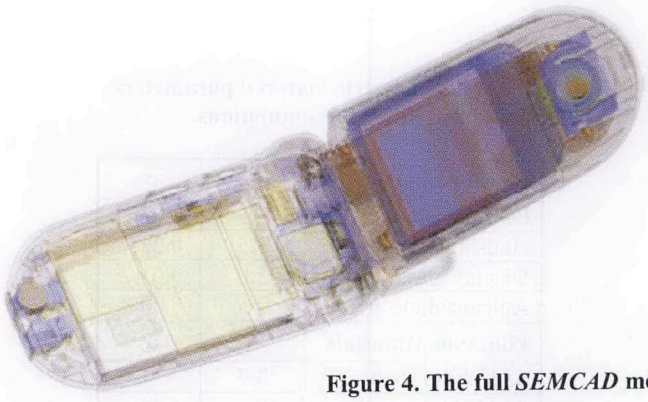

Figure 4. The full *SEMCAD* model of the phone.

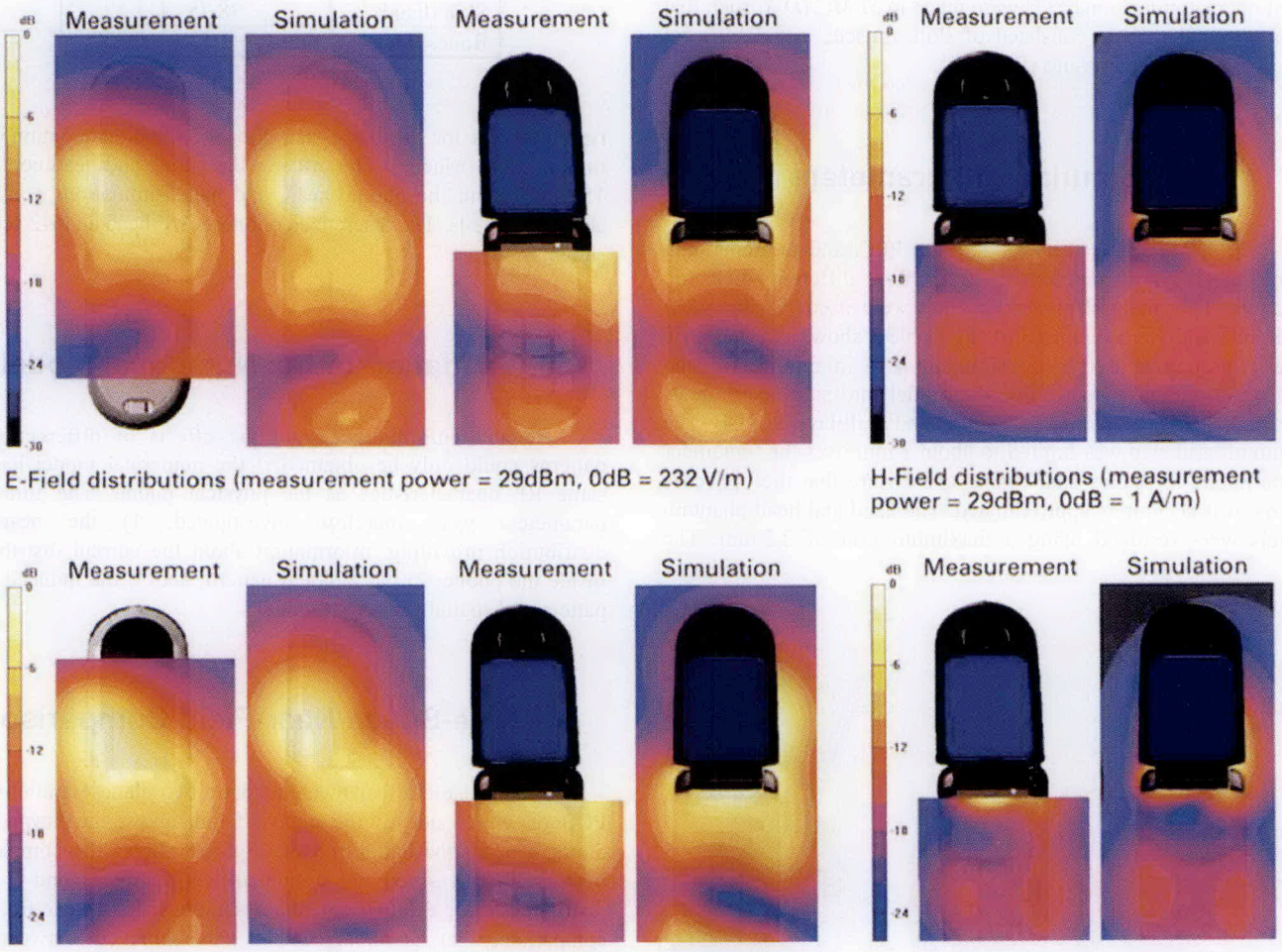

Figure 8. A comparison between simulation and measurement of the free-space E and H fields for antenna assemblies ant_A (top) and and_B (bottom).

approximately 1000 subparts, including almost all integrated circuits on the printed-circuit board (PCB). In addition, two different antenna assemblies were provided: the first antenna (ant_A) was a stretched helix, while the second (ant_B) was a parallel helix combination. The model was imported and modified to obtain the RF representation of the phone, i.e., whereby isolated components with dimensions of less than 1 mm^3 were removed, and special attention was placed on the antennas, including the feed point, flexible printed-circuit board, battery, connectors, shielding, components, housing, etc. Additional modifications were made to the PCB such that it was represented by a multilayered structure (three 120 μm PEC layers, two dielectric layers) for more accurate representation of the physical losses that occurred in the PCB (Figure 3). The full model that was used in the *SEMCAD X* simulations is shown in Figure 4. This process, lasting only a few hours, was verified by disassembling one of the physical phones provided by the manufacturer.

5.2 Simulation Phantom Models

The SAM head phantom, standardized by [7] for OTA performance testing, was used, since it provides high repeatability and the possibility for validation by measurements [22]. The three hand positions, as defined by the manufacturer as having a significant influence on the device's over-the-air performance are shown in Figure 5. The hand models were generated using *Poser*® and exported as `.3DS` CAD files (Figure 6). Further modifications based on anatomical data [23] were made in *SEMCAD X*, such that the final hand models consisted of skin, muscle, and significant finger and wrist bone tissues (Figure 7).

5.3 Simulation Parameters

All metallic parts were modeled as PEC, and the remaining phone parts were represented using five different dielectric materials. The material parameters that were used for the SAM head and hand were defined in [24]. Table 2 shows the dielectric material properties used in the simulations. A minimum grid step of 120 μm was used to resolve the model into significant areas, e.g., the helical antenna, feed structure, and multilayered PCB. The maximum grid step was limited to about 1 mm over the remainder of the phone to reduce stair-casing and ensure that the dielectric volume was accurately approximated. The hand and head phantom models were resolved using a maximum grid of 2.2 mm. The resulting grid for the free-space phone simulations contained 7.8 million cells (Mcells). The grid for the phone and head contained 15 Mcells, and the phone, head, and hand simulations contained about 19 Mcells. The discretized phone, SAM head and H2 setup is shown in Figure 7.

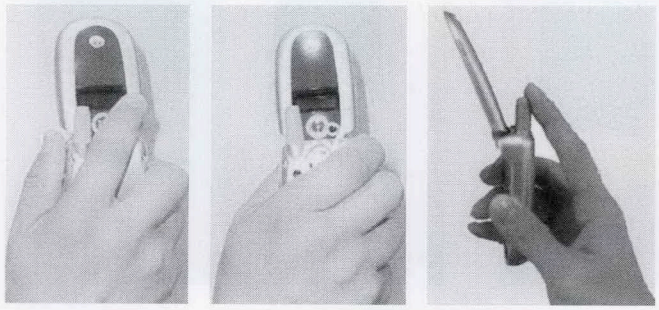

Figure 5. Real hand positions that have a significant influence on the performance of the device.

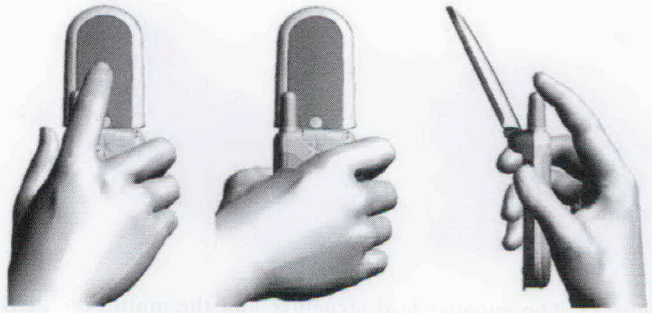

Figure 6. The CAD representations of the hands for the simulations: H1 (left), H2 (middle), and H3 (right).

Table 2. Dielectric material parameters used for the simulations.

Phone Materials	ε_r	σ
PCB dielectric	4.5	0.07
Housing parts	3.5	0.025
Display glass	3.0	0.01
Antenna dielectric	2.5	0.0045
Phantom Materials	ε_r	σ
SAM head shell	3.7	–
SAM head liquid	39	1.42
Muscle (hand)	53.44	1.385
Skin (hand)	38.75	1.22
Bones (hand)	11.73	0.289

6. Validation of the Numerical Model

Reliable information about the effects of different usage patterns could only be obtained if the numerical model had the same RF characteristics as the physical phone. The following parameters were therefore investigated: 1) the near-field distribution providing, information about the current distribution inside the phone; 2) the far-field pattern; and 3) the induced SAR pattern and spatial peak SAR values.

6.1 Free-Space Near-Field Comparison

E- and H-Field scans were made in two planes parallel to the PCB on either side of the phone, 5 mm above the keypad and 5 mm beneath the battery cover. Figure 8 shows the comparison between the measured and simulated data for the E- and H-Field distributions for the two antenna assemblies. It is clear from the comparison that good agreement was achieved between the measured and simulated near-field distributions. The slight differences were well within the uncertainties associated with the two platforms.

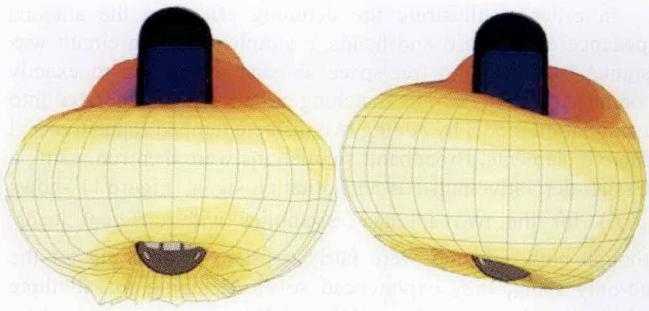

Figure 9. A three-dimensional comparison of the simulated (right) and measured (left) free-space radiation patterns.

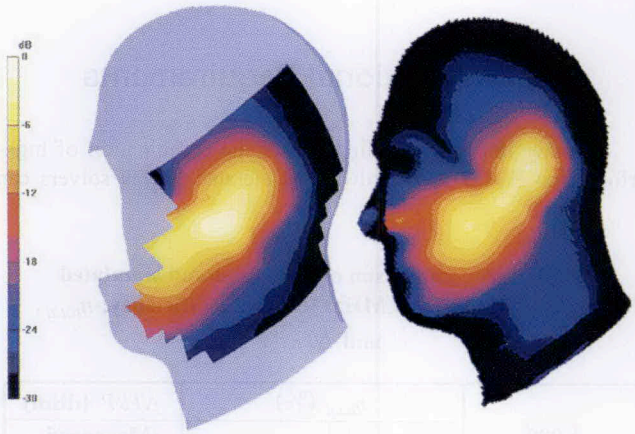

Figure 10. The SAR distribution: measurement (left) and simulation (right), normalized to the same value.

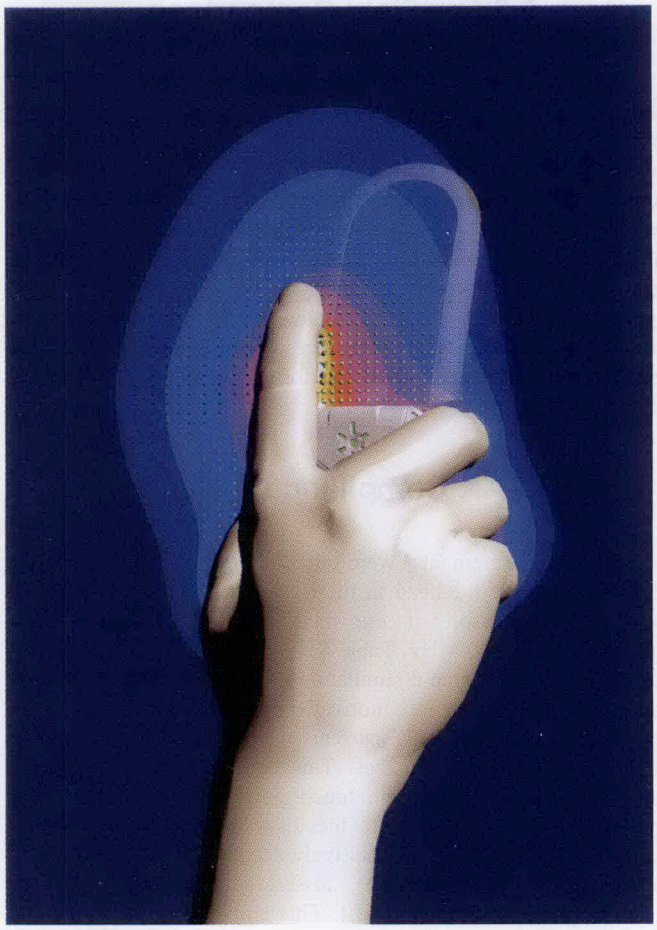

Figure 12. The distortion of the reactive near-field (E field) of the phone-antenna system by the presence of the hand (H3).

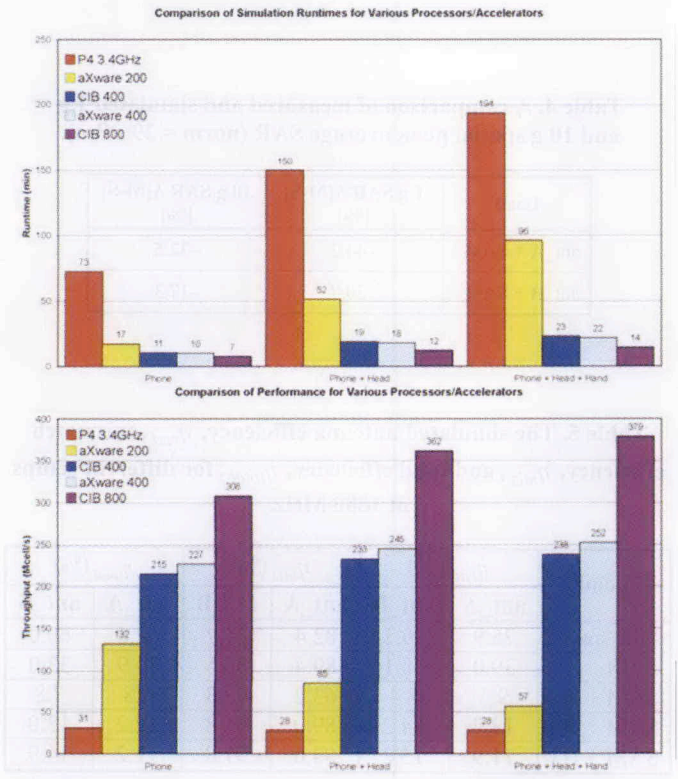

Figure 13. Computational requirements: the simulation times (top) and average computational speeds (bottom) for simulating the three structures using five different hardware configurations: 1) a typical P4 3.4 GHz desktop PC; 2) and 4) hardware accelerator cards; and 3) and 5) Cluster-in-a-Box (CIB) workstations, which were equipped with parallel combinations of two aXware cards with different speeds.

6.2 Far-Field Comparison

Far-field measurements were made in terms of efficiency, total radiated power (TRP), and radiation pattern. The values were compared for simulations of the free-space phone and for the phone against the head in the standard touch position [7]. Table 3 shows a list of the radiation efficiency and total radiated power, and Figure 9 shows a comparison of the measured and simulated three-dimensional radiation patterns. It was clear from the comparisons that good agreement was also achieved for the significant measured and simulated far-field performance parameters. The slight differences were well within the uncertainties associated with the platforms.

6.3 SAR Compliance Validation

SAR measurements were also performed for the phone positioned against the head in the right touch position. Figure 10 shows a comparison of the measured and simulated SAR distributions at 1880 MHz. Table 4 shows the differences between the measurement (M) and simulation (S) of the peak spatial SAR values. Closer examination, motivated by the differences obtained, revealed that substantial RF currents were coupled to the flexible PCB, amplified by resonances. This caused unnecessary losses when the phone was in the touch position, due to the close proximity of these currents to the lossy tissue [25]. Employing simple measures, such as capacitively decoupling the PCB, would substantially reduce these losses and strengthen the electromagnetic immunity (EMI). This emphasizes the value and need for employing simulation and measurement tools simultaneously.

7. Results

At this point in the study, a comprehensive validation of the numerical phone model had been completed. This achieved sufficient confidence to continue to investigate the effect of the different numerical hand models on the over-the-air performance of the device. The objective was to detect if either of the proposed antennas could lead to unacceptable performance impairment under loaded conditions. The total efficiency was considered in terms of the antenna efficiency and mismatch efficiency (since all metal parts were simulated as PEC, no metallic losses were considered in this definition):

$$\eta_{total} = \eta_{mis}\eta_{rad}, \qquad (1)$$

where η_{rad} is the antenna radiation efficiency, and $\eta_{mis} = \left(1 - |S_{11}|^2\right)$ is the mismatch efficiency.

Table 5 highlights the effect of the absorbing bodies in the vicinity of the close near field of the phone in terms of decreased radiation efficiency and detuning of the antenna's impedance. The results in Table 3 and Table 5 show the best-case performance, given that the different load impedances seen by the output stage of the power amplifier could lead to much lower power being supplied to the antenna, resulting in further reductions in total radiated power.

In order to illustrate the detuning effect on the antenna impedance of the head and hands, a simple matching circuit was designed to match the free-space antenna impedance to exactly 50 ohms at 1880 MHz. The matching circuit was incorporated into the simulation model by adding two discrete lumped capacitive and inductive elements. Broadband simulations were then run, using a Gaussian-derivative pulse as an excitation signal. Figure 11 shows $S_{11}(f)$ for the two antenna assemblies with different loads. Although both antennas were fairly resistant to detuning for the head-only setup, they experienced severe detuning for all three head-plus-hand setups. Hands H1 and H3 were characterized by more severe detuning, due to the close proximity of the index finger to the antenna. The overall combination of reduced efficiency and detuning effects were more pronounced for the ant_A assembly. Figure 12 illustrates the distortion of the reactive near-field (E field) of the phone-antenna system by the presence of the hand (H3).

8. Computational Requirements

Another important finding is that the combination of high-performance FDTD and hardware-accelerated FDTD solvers can

Table 3. A comparison of measured and simulated performance at 1880 MHz: Radiation efficiency, η_{total}, and ΔTRP.

Load	η_{total} (%)		ΔTRP (dBm)
	Measured	Simulation	(Measured – Simulation)
ant_A	71.3	62.6	0.84
ant_A + SAM	33.3	34.9	0.06
ant_B	66.4	60.0	0.71
ant_B + SAM	39.6	33.0	1.05

Table 4. A comparison of measured and simulated 1 g and 10 g spatial peak average SAR (norm = 29 dBm).

Load	1 g SAR Δ[M-S] [%]	10 g SAR Δ[M-S] [%]
ant_A + SAM	–44.2	–32.5
ant_B + SAM	–30.7	–17.3

Table 5. The simulated antenna efficiency, η_{rad}, mismatch efficiency, η_{mis}, and total efficiency, η_{total}, for different setups at 1880 MHz.

Load	η_{rad} (%)		η_{mis} (%)		η_{total} (%)	
	ant_A	ant_B	ant_A	ant_B	ant_A	ant_B
Free space	75.9	79.2	82.4	75.7	62.6	60.0
SAM	39.0	38.1	89.4	86.5	34.9	33.0
SAM + H1	9.1	8.4	63.2	92.8	5.8	7.8
SAM + H2	13.7	14.2	89.0	91.8	12.2	13.0
SAM + H3	11.9	15.2	94.0	97.8	11.2	14.9

Table 6. Computational requirements for the phone in free space and beside the SAM phantom setup.

Load	Frequency (MHz)	Grid (Mcells)	ΔS_{min} (μm)
Free space	1880	7.8	120
SAM	1880	14.9	120
SAM + H1	1880	19	120

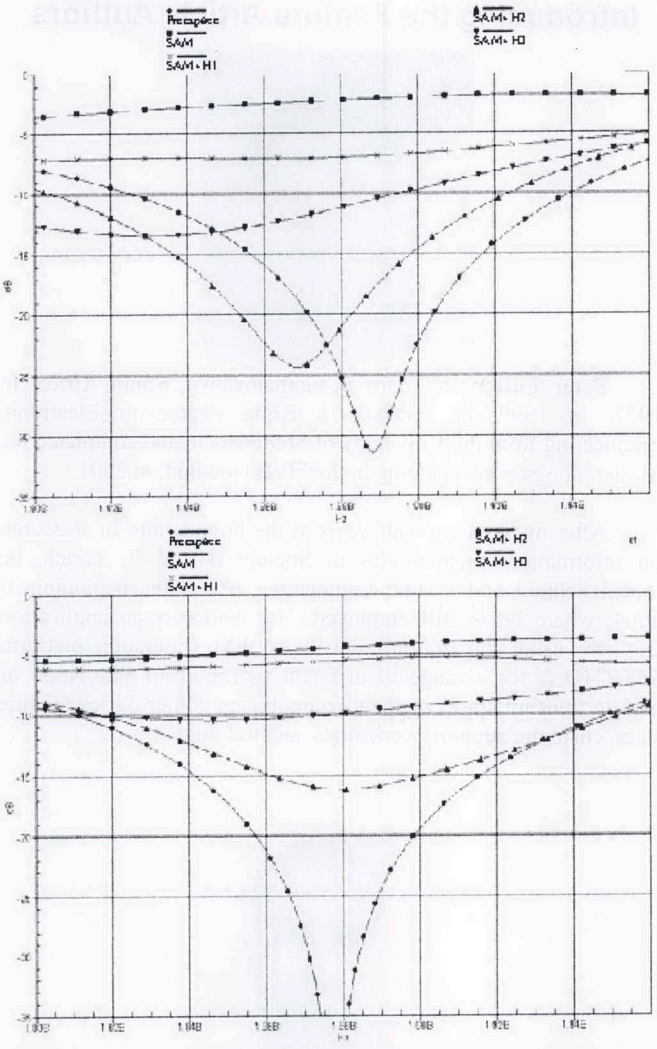

Figure 11. S_{11} **for the ant_A (top) and ant_B (bottom) antenna assemblies.**

provide greatly reduced modeling and simulation times. The data importation, modeling, and modifications required about three hours. The simulations for free-space, SAM, and SAM-plus-H1 structures on the different platforms took as little as seven minutes (phone only) to 14 minutes (phone, head, hand), using hardware acceleration. Figure 13 illustrates the speed comparison. Table 6 gives an overview of the grid sizes for the three simulations.

9. Conclusions

This study demonstrated the latest progress in CEM, and showed that enhanced FDTD tools are suitable for supporting engineers in the analysis, design, and optimization of complex transmitters, such as commercial multi-band mobile phones. The effects of different usage patterns on the RF performance could be effectively, accurately, and reliably assessed, even before the physical phone model was built. The SAR comparison also demonstrated the great potential of combined numerical and experimental analysis. Device performance can be substantially improved with simple measures, such as the RF decoupling of certain phone parts that cause unnecessary losses and exposure, thereby enhancing the EMI potential.

10. References

1. A. Taflove and S. C. Hagness, *Computational Electrodynamics – The Finite Difference Time Domain Method, 3rd Edition*, Norwood, MA, Artech House, 2005.

2. K. Yee, "Numerical Solution of Initial Boundary Value Problems Involving Maxwell's Equations in Isotropic Media," *IEEE Transactions on Antennas and Propagation*, **AP-14**, 1966, pp. 302-307.

3. M. Jensen and Y. Rahmat-Samii, "EM Interaction of Handset Antennas and a Human in Personal Communications," *Proceedings of the IEEE*, **83**, January 1995, pp. 7-17.

4. M. Okoniewski and M. Stuchly, "A Study of the Handset Antenna and Human Body Interaction," *IEEE Transactions on Microwave Theory and Techniques*, **MTT-44**, October 1996, pp. 1855-1864.

5. M. Burkhardt, N. Chavannes, K. Pokovic, T. Schmid, and N. Kuster, "Study on the FDTD Performance for Transmitters in Complex Environments," *Proceedings of the ICECOM*, Dubrovnik, October 1997, pp. 83-86.

6. N. Chavannes, R. Tay, N. Nikoloski, and N. Kuster, "Suitability of FDTD Based TCAD Tools for RF Design of Mobile Phones," *IEEE Antennas and Propagation Magazine*, **45**, December 2003, pp. 52-66.

7. CTIA Certification, "Test Plan for Mobile Station Over the Air Performance," CTIA Wireless Association, April 2005.

8. S. Benkler, N. Chavannes, and N. Kuster, "A New 3-D Conformal PEC FDTD Scheme with User-Defined Geometric Precision and Given Stability Criterion," *IEEE Transactions on Antennas and Propagation*, **AP-54**, June 2006, pp. 1843-1849.

9. N. Chavannes and N. Kuster, "A Novel 3-D CPFDTD Scheme for Modeling Grid Non-Conformally Aligned Transmitter Structures," *IEEE Transactions on Antennas and Propagation*, **AP-52**, May 2004, pp. 1324-1334.

10. H. Songoro, S. Benkler, N. Chavannes, and N. Kuster, "On the Real World Performance of ADI-FDTD," 2005 IEEE International Symposium on Antennas and Propagation and USNC/URSI National Radio Science Meeting, Washington DC, USA, July 3-8, 2005.

11. S. Benkler, N. Chavannes, and N. Kuster, "Versatile Approach of Incorporating Subcell Models into the 3-D ADI-FDTD Method," *IEEE Transactions on Antennas and Propagation*, submitted 2006.

12. E. Neufeld, T. Samaras, N. Chavannes, and N. Kuster, "New Model to Simulate EM Induced Temperature Distributions and the Influence of Blood Flow," 28th Annual Meeting of the Bio-Electromagnetics Society, Cancun, Mexico, June 2006, pp. 430-431.

13. R. Schneider, S. Krakiwsky, L. Turner, and M. Okoniewski, "Advances in Hardware Acceleration for FDTD," in A. Taflove (ed.), *Computational Electrodynamics: The Finite-Difference Time-Domain Method, Third Edition*, Norwood, MA, Artech House, 2005, Chapter 20.

14. F. Nunez and A. Skrivervik, "GA Optimization of Terminal Antennas by the Estimation of the Population Density of Probability Using Dependency Trees," 2004 IEEE International Symposium on Antennas and Propagation and USNC/URSI National Radio Science Meeting, Monterey, USA, June 2004.

15. S. Benkler, N. Chavannes, and N. Kuster, "Mastering Conformal Meshing for Complex CAD Based C-FDTD Simulations," *IEEE Antennas and Propagation Magazine*, accepted for publication.

16. N. Chavannes, "Nonuniform Grids, Nonorthogonal Grids, Unstructured Grids, and Subgrids," in A. Taflove (ed.), *Computational Electrodynamics: The Finite-Difference Time-Domain Method, Third Edition*, Norwood, MA, Artech House, 2005, Section 11.8.

17. S. Schild, N. Chavannes, and N. Kuster, "New FDTD Scheme for the Modeling of Arbitrarily Curved Thin Conductive Sheets," 2006 IEEE International Symposium on Antennas and Propagation and USNC/URSI National Radio Science Meeting, Albuquerque, NM, USA, July 2006.

18. SEMCAD X, "Reference Manual for the SEMCAD X Simulation Platform for Electromagnetic Compatibility, Antenna Design and Dosimetry," SPEAG-Schmid & Partner Engineering AG, version 11.0, July 2006, http://www.semcad.com.

19. IEEE 1528/D1.2, "Recommended Practice for Determining the Spatial-Peak Specific Absorption Rate (SAR) in the Human Body Due to Wireless Communications Devices: Measurement Techniques," Piscataway, NJ, IEEE, April 2003.

20. K. Poković, "Advanced Electromagnetic Probes for Near-Field Evaluations," PhD dissertation, Diss. ETH Nr. 13334, Zurich, 1999.

21. IEC 62209 Part 1, "Human Exposure to Radio Frequency Fields from Handheld and Body-Mounted Wireless Communication Devices – Human Models, Instrumentation and Procedures, Part 1: Procedure to Determine the Specific Absorption Rate (SAR) for Handheld Devices Used in Close Proximity to the Ear (Frequency Range of 300 MHz to 3 GHz), Geneva, Switzerland, February 2005.

22. E. Ofli, N. Chavannes, and N. Kuster, "The Uncertainties and Repeatability Limitations of Transmitter and Receiver Performance Assessments Posed by Head Phantoms," *Proceedings of the 2006 IEEE International Workshop on Antenna Technology: Small Antennas and Novel Metamaterials (IWAT)*, March 2006, pp. 349-352.

23. http://www.gwc.maricopa.edu/class/bio201/.

24. FCC, "Evaluating Compliance with FCC Guidelines for Human Exposure to Radiofrequency Electromagnetic Fields," Supplement C to OET Bulletin 65, Washington, DC, FCC, June 2001.

25. N. Kuster and Q. Balzano, "Energy Absorption Mechanism by Biological Bodies in the Near Field of Dipole Antennas above 300 MHz," *IEEE Transactions on Vehicular Technology*, **VT-41**, February 1992, pp. 17-23.

Introducing the Feature Article Authors

Peter Futter was born in Grahamstown, South Africa, in 1977. In 1999, he received a BEng degree in Electronic Engineering from the University of Stellenboch, and completed his Master's degree, specializing in the FDTD method, in 2001.

After one-and-one-half years at the Foundation for Research on Information Technologies in Society (IT'IS) in Zurich, he joined Schmid and Partner Engineering AG at the beginning of 2004, where he is still employed. His works as an application engineer using the in-house-developed EM simulation platform *SEMCAD X* for a range of different topics, from simulation of mobile transmitters to medical technologies. Other duties include sales, customer support, workshops, and training.

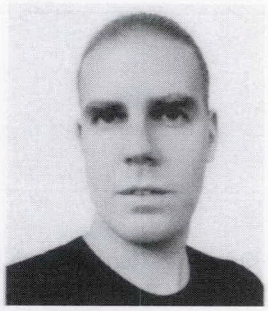

Nicolas Chavannes was born in Bern, Switzerland, in April 1972. He received the MS and PhD degrees in Electrical Engineering from the Swiss Federal Institute of Technology (ETH), Zurich, Switzerland, in 1998 and 2002, respectively. In 1996, he joined the Bioelectromagnetics/EMC Group (BIOEM/EMC) at ETH Zurich, where he was involved in computational electrodynamics and related dosimetric applications. From 1998 to 2002, he was with the Laboratory for Electromagnetic Fields and Microwave Electronics (IFH) as well as the Laboratory for Integrated Systems (IIS), both located at ETH Zurich. There, his research activities were focused on the development of FDTD local-refinement techniques and their application to numerical near-field analysis. In late 1999, he joined the Foundation for Research on Information Technologies in

Society (IT'IS), Switzerland, where he is currently in charge of the development and extension of a simulation platform targeted for antenna modeling and MTE design in complex environments, dosimetry, and optics applications. In early 2002, he joined Schmid & Partner Engineering AG (SPEAG), Zurich, as head of the software R&D team. His primary research interests include the development, implementation, and application of computational modeling and simulation techniques to electromagnetics in general, and antennas, as well as bioelectromagnetic interaction mechanisms, in particular.

Roger Yew-Siow Tay received the BS and MS degrees in Electrical Engineering from the University of Massachusetts, Lowell, in 1983 and 1985, respectively, and the PhD degree from the Swiss Federal Institute of Technology (ETH), Zurich, Switzerland, in 1997. He is currently a Distinguished Member of the Technical Staff at Motorola's Global Center of Excellence in Singapore. He leads the Advance Electrical Engineering team in the design and development of cellular phones. He set up the Electromagnetics Laboratory in the Motorola Singapore facility, and installed the first SAR measurement system based on the DASY system in Southeast Asia. His interests include antennas for personal-communication devices, antenna metrology, dosimetry, and techniques to modularize transceiver systems for wireless communication devices. He holds eight US patents and several pending patents, and has contributed papers in many journals and conferences. Dr. Tay is a member of the IEEE Antennas and Propagation, Vehicular Technology, Communications, and Electromagnetics Compatibility Societies. He is also a Committee Member of the Singapore Chapter of the IEEE EMC Society.

Mike Meili was born in Zug, Switzerland, in 1976. In 1999, after apprenticeship as an electronic engineer, he worked as an intern at Laurier, Inc., in New Hampshire, USA, for development and support of die sorting systems. After returning to Switzerland in 2001, he started working with V-Zug AG in Zug, Switzerland. Employed in the R&D department, he was involved in developing washing machines and dryers. In 2004, he joined Schmid & Partner Engineering AG (SPEAG), Zurich, as an RF Technician. His fields of work include calibrating, support, installation, and developing work for SPEAG projects and machines.

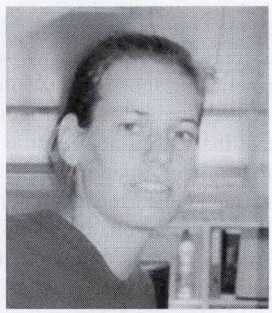

Anja Klingenböck was born in Baden, Switzerland, in 1973, and studied Environmental Sciences at ETH Zurich, where she graduated in 1999. She joined the Foundation for Research on Information Technologies in Society in November 2001, initially working on a discretization of the Visible Human model. She has also worked on various projects dealing with animal and human phantoms for simulations in *SEMCAD X*, and was extensively involved in the e-learning project called Virtual Excursion for the Geobotanical Institute of ETH.

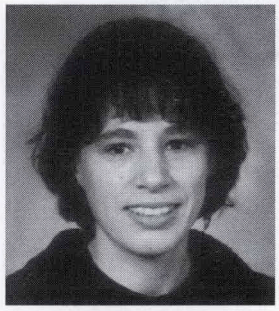

Katja Pokovic, born in 1968 in Dubrovnik, Croatia, received her BS and MS in Electrical Engineering from the University of Zagreb, Croatia. She received her PhD from the Swiss Federal Institute of Technology (ETH), Zurich, Switzerland. From 1993 to 1995, she worked at the Laboratory for High Frequency Techniques, FER-Zagreb, as an assistant and technical secretary of the European COST244 project Biomedical Effects of Electromagnetic Fields. In June 1995, she joined the BIOEM/EMC group at the Laboratory for Electromagnetic Fields and Microwave Electronics, ETH Zurich, where she conducted her PhD work on optimized probe designs for near-field evaluations in the mobile frequency range. Since October 1999, Katja has been employed at SPEAG as Laboratory Director. Katja also advises SPEAG customers in all areas of near-field evaluation and optimization, and represents SPEAG in standardization committees.

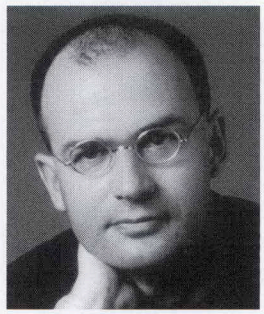

Niels Kuster was born in Olten, Switzerland, in 1957. He received the MS and PhD degrees in Electrical Engineering from the Swiss Federal Institute of Technology (ETH), Zurich, Switzerland.

In 1993, he became a Professor with the Department of Electrical Engineering, ETH. In 1992, he was an Invited Professor with the Electromagnetics Laboratory, Motorola, Inc., Fort Lauderdale, FL, and in 1998, with the Metropolitan University of Tokyo, Tokyo, Japan. In 1999, he became Director of the Foundation for Research on Information Technologies in Society (IT'IS), Zurich, Switzerland. His research interests are currently focused on the area of reliable on/in-body wireless communications and related topics. This includes measurement technology and computational electrodynamics for evaluation of close near-fields in complex environments, safe and reliable wireless communication links within the body or between implanted devices and the outside for biometrics applications, development of exposure setups and quality control for bio-experiments evaluating interaction mechanisms, therapeutic effects, as well as potential health risks, and exposure assessments.

Dr. Kuster is a member of several standardization bodies, and has consulted with several government agencies on the issue of the safety of mobile communications. He also served on the boards of scientific societies, research management councils for governments, and editorial boards.